# Effect of Center of Gravity and Moment of Inertia in a Free-Flight Environment Using a Rubber Balloon

By Hideto Takasawa, [1] Tadayuki Yoshio, [2] Haruka Yamamoto, [3] Sota Takano, [2] Ryou Miyashita, [2] Takahiro Miki, [4] Yusuke Takahashi, [2] Yasunori Nagata [1] and Kazuhiko Yamada[1]

[1]*Institute of Space and Astronautical Science, JAXA, Sagamihara, Japan*
[2] *Division of Mechanical and Space Engineering, Hokkaido University, Sapporo, Japan*
[3] *Department of Materials Science and Technology, Tokyo University of Science, Katsushikaku, Japan*
[4] *Department of Applied Mechanics and Aerospace Engineering, Waseda University, Shinjuku, Japan*

(Received March 10th, 2023)

A low ballistic coefficient, thin aeroshell capsule has been proposed to mitigate aerodynamic heating during reentry from deep space. Since the capsule is parachute-less, it must maintain an appropriate attitude during flight to achieve sufficient aerodynamic deceleration and mitigate the impact upon landing. To evaluate the effect of mass properties for aerodynamic stability in the low-speed regime, two capsules with different center of gravity positions were released and their free-flight behavior was recorded. The capsules, each 0.8 m in diameter and approximately 2 kg in mass, were dropped from an altitude of 25 km using a rubber balloon. Analyses of acceleration, angular velocity, and pressure histories revealed that the dominant frequencies were associated with rotational oscillations caused by static aerodynamic moments and translational oscillations induced by unsteady flow phenomena. Additionally, evaluation of the time history of capsule energy suggested that while shifting the center of gravity aft increased the tendency toward instability by approaching the aerodynamic center. However, in both capsules, oscillations were suppressed at lower altitudes. This suppression may be attributed to the effects of the additional moment of inertia as atmospheric density increased.

**Key Words:** Dynamic Stability, SRC, Balloon Experiment

## Nomenclature

| | | |
|---|---|---|
| $C_B$ | : | ballistic coefficient |
| $C_D$ | : | drag coefficient |
| $C_{m\alpha}$ | : | pitching moment slope |
| $D$ | : | length, m |
| $f$ | : | frequency, $s^{-1}$ |
| $H$ | : | Hamiltonian, J |
| $I$ | : | moment of inertia, kg $m^2$ |
| $M$ | : | Mach number |
| $m$ | : | mass, kg |
| $p$ | : | generalized momentum |
| $q$ | : | generalized coordinate |
| $S$ | : | projected area, $m^2$ |
| $u$ | : | velocity, m/s |
| $\rho$ | : | density, kg/$m^3$ |
| $\omega$ | : | angular velocity, rad/s |

## 1. Introduction

Sample return missions to gain new scientific insights into the formation of the solar system and the origins of life. Currently, sample return missions from the Martian system, such as MMX, are underway, and in the future, missions targeting the Saturnian system beyond the snow line will be required. Assuming a sample return mission from the Saturnian system, the reentry velocity into Earth's atmosphere could reach as high as 15 km/s. Consequently, the return capsule would be subjected to a severe aerodynamic heating environment.

To mitigate this issue, a heat-mitigation approach utilizing a low ballistic coefficient thin aeroshell capsule for the Deep Space Sample Return Capsule (DS-SRC)[1], as illustrated in Figure 1, has been proposed. This capsule achieves high aerodynamic deceleration performance and is designed to be lightweight by eliminating the need for parachutes and avionics. Furthermore, its large-diameter aeroshell with a 60-degree half-angle enables deceleration to begin at high altitudes where atmospheric density is low. These features contribute to reducing the capsule's velocity at the altitude where peak heating occurs in conventional capsules.

A parachute-free system also simplifies the reentry sequence and reduces mission risks such as parachute deployment. Additionally, the landing velocity of this capsule is estimated to be below 20 m/s, and the impact at landing is mitigated using shock-absorbing materials.

One of the issues during atmospheric reentry is aerodynamic instability. This is the phenomenon in which the capsule's attitude diverges due to aerodynamic forces during free flight. Such instability disturbs sufficient aerodynamic deceleration or achieving a proper landing attitude. In fact, during the Hayabusa2 mission[2], an unexpected increase in oscillatory motion was observed in the subsonic regime. Similar behavior has also been identified in other capsules[3,4]. While it is known that various parameters affect instability[5], it is particularly important to clarify how each parameter affects the instability in the low-speed regime, where divergence phenomena have been observed, and to understand the mechanisms behind such divergence.

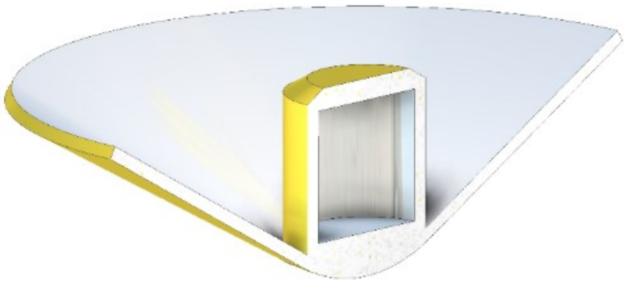

Fig. 1. Illustration of thin aeroshell type capsule (DS-SRC).

To investigate this instability, various evaluation methods such as wind tunnel experiments and computational fluid dynamics (CFD) analyses have been employed. When one degree-of-freedom (1-DOF) oscillation tests have been conducted in wind tunnels, the Hayabusa-type capsule was considered stable in subsonic flow[6]. However, as mentioned earlier, the Hayabusa2 capsule exhibited instability, suggesting the need for testing with higher degrees of freedom and experimental data with minimal interference from support structures, such as stings. While numerical simulations have the potential to find methods to solve these issues, the oscillations observed in free flight occur in the order of one second. Capturing transient behavior requires time-accurate simulations spanning approximately ten seconds, which entails significant computational cost.

The present study conducts a free-flight experiment using a rubber balloon to evaluate the effect of mass properties on attitude motion. We refer to these flight tests as the Rubber Balloon Experiment for a Reentry Capsule with a Thin Aeroshell (RERA). In particular, the experiment aims to collect flight data in the subsonic regime, where divergent oscillations are expected to occur. Although the number of achievable free-flight tests is limited and the data obtained is sparse, the experiment enables evaluation under full six-degree-of-freedom conditions. Furthermore, the data can serve as valuable reference for refining wind tunnel tests and improving numerical analysis methods.

## 2. Overview of RERA-2, -4

In this experiment, we evaluate the effects of mass properties on the attitude motion of a thin aeroshell capsule during free flight in the subsonic regime. Two types of capsules with different mass properties, that is, the center-of-gravity (CG) locations, were used. Due to the shift in CG, the moment of inertia (MOI) also differs between the two configurations. It should be noted that the test capsules differ from the actual reentry capsule design, DS-SRC (0.8 m diameter, 10 kg mass), which is intended for practical reentry missions.

### 2.1. RERA capsule

Compared to the DS-SRC, the RERA capsules are full-scale but significantly lighter, as the outer shell is made of Expanded Polystyrene (EPS). Table 1 summarizes the mass properties of each RERA capsule. The drag coefficient $C_D$ was adopted from values reported in previous studies[7].

Table 1. Specifications of the capsules.

| | RERA-2 | RERA-4 |
|---|---|---|
| Mass, kg | 1.98 | 1.79 |
| Diameter, m | 0.8 | 0.8 |
| Height, m | 275 | 405 |
| CG, mm | 147.8 | 244.5 |
| MOI through CG around (x, y, z), $10^{-2}$ kg m$^2$ | (2.3, 2.3, 3.7) | (2.8, 2.8, 2.8) |
| Ballistic coefficient ($C_D$ = 0.96), kg/m$^2$ | 4.10 | 3.71 |

The MOIs of the onboard equipment were directly measured, while the MOIs of the EPS components were estimated from their volume derived by CAD and mass. The order of magnitude of the MOIs for RERA is approximately one-tenth that of DS-SRC. Additionally, to reduce weight, the EPS used for RERA-4 was of lower density, resulting in different trends in the roll-direction MOI compared to RERA-2. A comparison between RERA-2 and RERA-4 reveals a 12% difference in CG location relative to the capsule diameter, and approximately a 20% difference in pitch and yaw MOIs.

The external appearance and schematic of the RERA-4 capsule are shown in Figures 2 and 3, respectively. The CG locations listed in Table 1 are expressed as coordinates with the capsule tip defined as the origin. The lateral offset of the CG from the central axis was less than 2 mm. The capsule's outer structure is composed of EPS, with onboard components housed in the rear cylindrical section. Only adhesive KE-60 (Konishi Co., Ltd.) was used for assembly. The transmission antenna was embedded in the front flare section for RERA-2 and in the rear cylindrical section for RERA-4. In RERA-4, the cylindrical section is taller to accommodate a rearward CG location. The rubber balloon used for the experiment was a TA-2000 model manufactured by TOTEX Corporation.

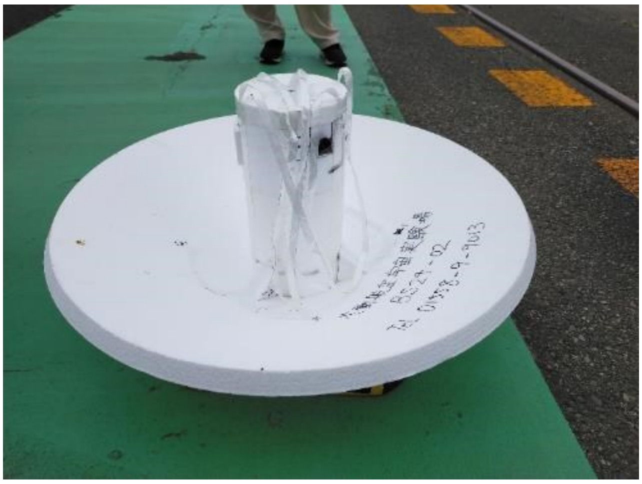

Fig. 2. External appearance of the RERA-4 capsule.

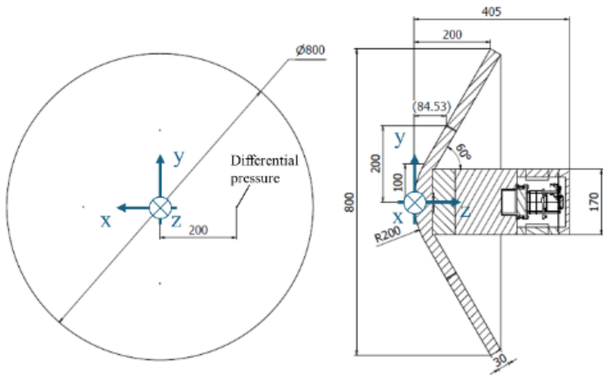


Fig. 3. A schematic of the RERA-4 capsule and object coordinate system.

## 2.2. Measurement system

A list of the onboard components is provided in Table 2. In this experiment, attitude data were measured using a 9-axis sensor. The sensor locations differed between the two capsules: in RERA-2, the attitude data were measured at (-6.9, 4.0, 192.8), and in RERA-4 at (-6.9, 4.0, 322.8). The sampling rates for each data set are summarized in Table 3. The dominant frequencies of oscillatory motion in pitch and yaw were estimated to be approximately 1 Hz; thus, a sampling rate of 100 Hz was sufficient to capture these motions. The absolute pressure is measured at the stagnation point, and differential pressures between the stagnation point and four locations on the forebody of the capsule, as shown in Fig. 3, are measured and used for attitude estimation.

Table 2. Onboard sensors.

| Sensor | Maker | Model number |
|---|---|---|
| 9-axis sensor (accelerometer, gyroscope, magnetometer) | Xsens | MTi-2 |
| GPS receiver | MIKROE | NEO-M9N |
| GPS antenna | Tallysman | TW1421 |
| Pressure gauge | Honey well | SSCDANN015PAAB5 (Absolute) HSCDRRN001NDAA5 (Differential) |
| Temperature transducer | Analog Devices | AD590 |
| Camera | OpenMV | OpenMV Cam H7 R2 |

Table 3. Sampling rate of measurements.

| Value | Sampling rate, Hz |
|---|---|
| Acceleration | 100 |
| Angular velocity | 100 |
| Magnetic field | 100 |
| GPS data | 10 |
| Pressure | 10 |
| Temperature | 10 |
| Imaging | 0.1 |

An overall view of the equipment is shown in Figure 4.

The U-TeCS is a data aggregation board developed for flight testing. The transmitter and data transmission antennas were provided by the JAXA Balloon Group. The battery (3B0075, Greatbatch), consisting of two cells connected in series, was selected from those used in previous balloon experiments. The equipment had a maximum diameter of 0.150 m, a height of 0.116 m, and a total mass of 1.3 kg. The aluminum plate directly beneath the GPS antenna and battery box were bonded to the inner wall of the EPS container.

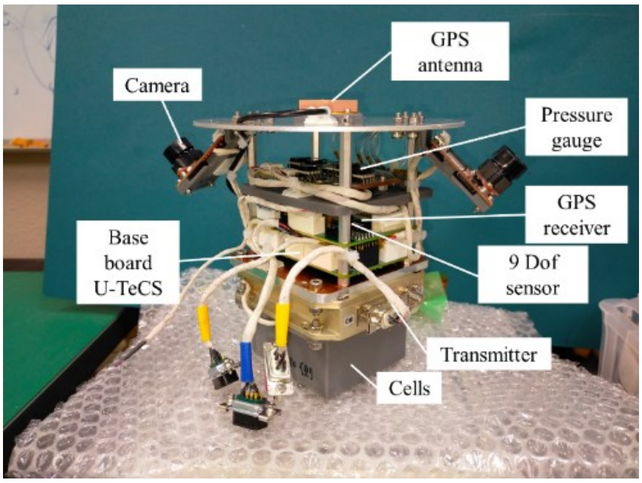


Fig. 4. Equipment in RERA-4 capsule.

# 3. Flight Results

In the RERA experiment, the capsule was lifted to an altitude of approximately 25 km by a small scientific balloon, similar to a radiosonde balloon, and then released to perform a free-flight descent. Free-flight data were collected over a duration of approximately 20 minutes until splashdown in the ocean.

## 3.1. Flight history

Figure 5 shows the velocity profiles of RERA-2 and RERA-4 at each altitude. Wind velocity data were obtained from the National Centers for Environmental Prediction (NCEP)[8), using the value corresponding to the closest available time in hourly intervals. The horizontal components of the wind velocity (latitude and longitude directions) were generally consistent with those of the RERA capsules, indicating that the vertical component dominated the relative velocity. This suggests that the RERA capsules, due to their low ballistic coefficient, were significantly affected by crosswinds and descended while experiencing lateral drift. In the following analysis, the vertical velocity component is used as the representative relative velocity with respect to the airflow.

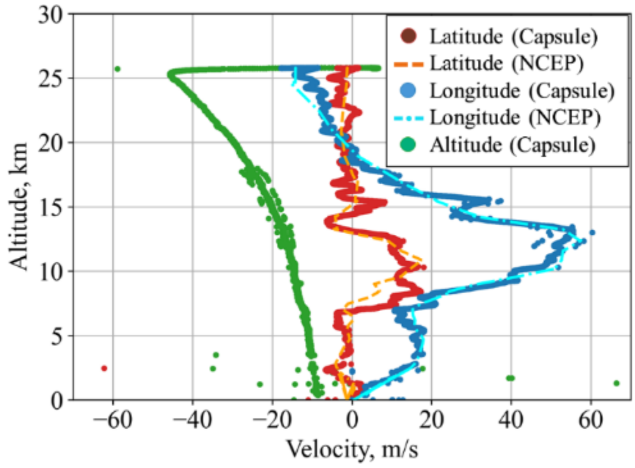


(a) RERA-2

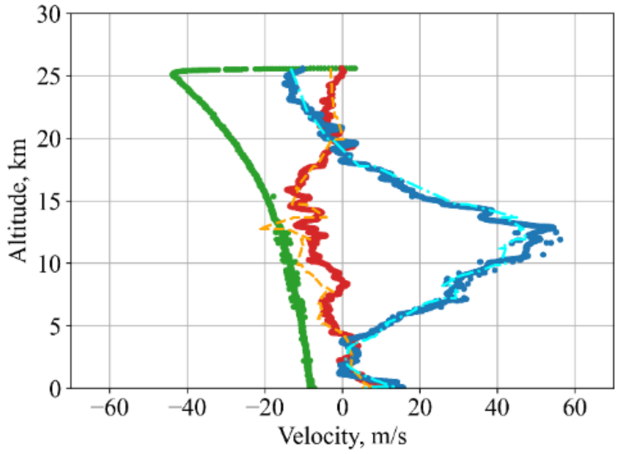


(b) RERA-4

Fig. 5. Velocity at each altitude calculated from GPS location history.

The initial condition of flight is listed in Table 4. Due to the difficulty in controlling the capsule's motion at the time of separation, significant differences were observed in the initial roll motion. However, as discussed in Section 3.2, the roll motion of the RERA capsule rapidly diminished, indicating that the aerodynamic inducing roll motion was relatively weak.

Table 4. Initial condition of flight.

| | RERA-2 | RERA-4 |
|---|---|---|
| Acceleration, m/s$^2$ | (0.42, 0.23, -10.69) | (0.02, -0.12, -9.00) |
| Angular velocity, deg/s | (9.7, -2,9, 85.9) | (3.7, 4.9, 23.87) |
| Altitude, km | 25.8 | 25.6 |

The Mach number and Reynolds number profiles for each capsule are shown in Figure 6. Since RERA-2 and RERA-4 have approximately the same ballistic coefficient, the velocity regimes experienced by both capsules were similar. During the free flight, the Reynolds number was on the order of $10^5$, and the Mach number remained below 0.15.

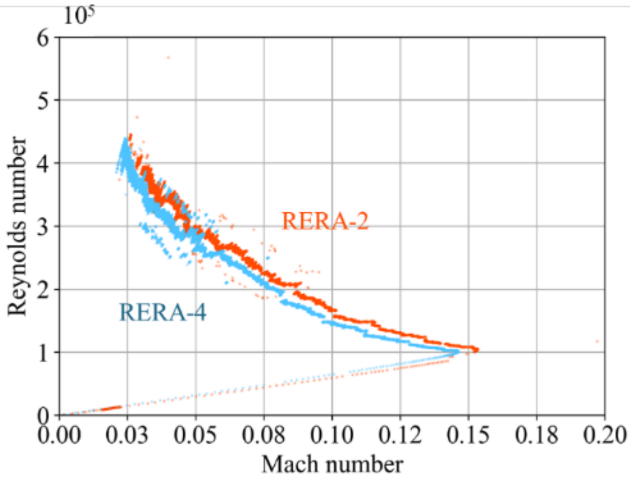


Fig. 6. Profile of Mach number versus Reynolds number based on measured flight data and analysis.

### 3.2. Attitude

Both the RERA-2 and RERA-4 capsules exhibited stable behavior throughout the descent, without any attitude divergence. This is further supported by the absence of divergence in the trajectory histories shown in Figures 5 and 6. In Section 3.2, we analyze the results of RERA-4 in detail, focusing on differences in acceleration, angular velocity, and pressure data compared to RERA-2.

#### 3.2.1. Acceleration

Figure 7-(a) shows the acceleration history of RERA-4. As seen in the figure, the Z-axis acceleration, which reflects gravitational acceleration when the attitude is stable, consistently remains around 10 m/s$^2$. This indicates that the capsule's attitude remained stable throughout the descent without divergence.

To capture the dominant dynamics associated with pitch and yaw oscillations (i.e., oscillations around the x and y axes), an Fast Fourier Transform (FFT) analysis was conducted on the x- and y-axis acceleration data at 10-second intervals. The results for the x-axis are presented in Figure 7-(b). Initially, oscillations with a frequency slightly below 1.5 Hz were dominant. Over time, the peak frequencies became more dispersed. Overall, oscillations below 1.5 Hz were predominant throughout the flight.

The oscillation frequency of capsule is estimated based on a simplified 1-DOF oscillation. Assuming that the capsule is primarily oscillated by the static aerodynamic moment, the oscillation frequency can be approximated using Equation (1)[9].

$$f = \frac{\omega}{2\pi} = \frac{1}{2\pi}\sqrt{\frac{-C_{m\alpha}\rho_\infty u_\infty^2 SD}{2I}} = \frac{1}{2\pi}\sqrt{\frac{-C_{m\alpha} mgD}{C_D I}} \quad (1)$$

Based on previous studies[10], the moment gradient $C_{m\alpha}$ at the CG of RERA-4 is estimated to be 0.131, and the drag coefficient $C_D$ is 0.964. Here, $m$ denotes the capsule mass,

$g$ is the gravitational acceleration, $D$ is the reference length, and $I$ is the moment of inertia. Using these values, the oscillation frequency $f$ is estimated to be approximately 1.3 Hz, suggesting that the observed spectral peak near 1.3 Hz is attributable to this rotational oscillation mode.

In addition, as time progresses, oscillation peaks begin to appear below 1 Hz. Previous studies[11)] on oscillation phenomena around discs have identified two typical unsteady phenomena: helical vortex shedding, where alternating vortices are formed due to flow separation near the shoulder, and bubble pumping, characterized by amplitude oscillations in the streamwise direction. The corresponding Strouhal numbers are estimated to be 0.12 and 0.02, respectively. Using the velocity in altitude direction during free flight and these Strouhal numbers, the expected frequencies for each phenomenon are plotted in Figure 7-(c). Unlike the rotational oscillation frequency, which remains constant during descent due to its dependence on dynamic pressure, these flow-induced oscillations decrease as the capsule decelerates, owing to their proportionality to the velocity. A qualitative comparison of the bubble pumping frequency trend with the FFT results in Figure 7-(b) reveals a consistent emergence of sub-0.5 Hz components over time.

Similar spectral analyses were conducted on angular velocity and pressure data in Sections 3.2.2 and 3.2.3. While no sub-0.5 Hz components were observed in the angular velocity spectra, pressure data clearly exhibited such low-frequency components. This discrepancy is consistent with the nature of bubble pumping, which induces translational oscillations in the flow direction. Hence, it affects acceleration and pressure signals but not angular velocity.

These observations collectively suggest that during free flight, the capsule experienced both rotational and flow-induced oscillations. Similar trends were also observed in the RERA-2 capsule.

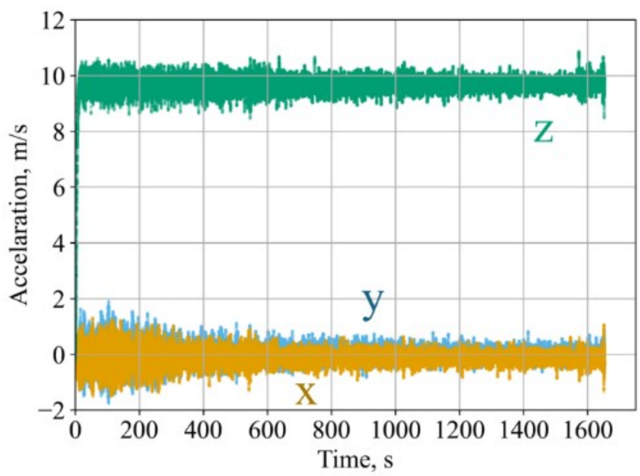


(a) Time history of acceleration in the body-axis directions (x, y, z).

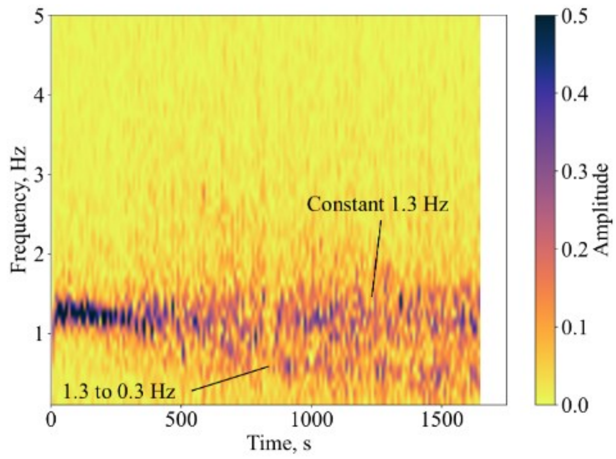


(b) Time history of frequency in x-axis acceleration.

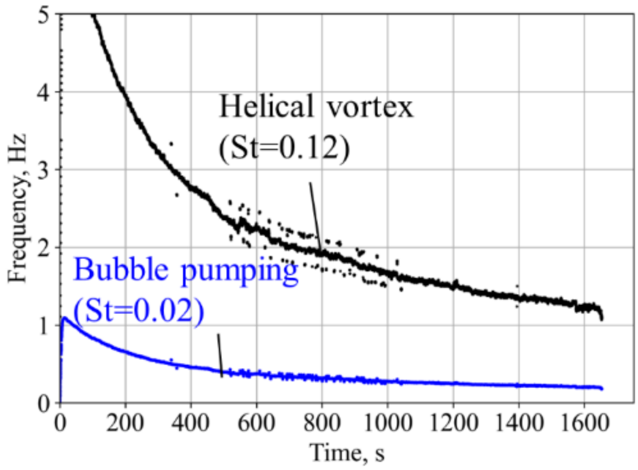


(c) Estimated frequency histories of helical vortex (St = 0.12) and bubble pumping (St = 0.02).

Fig. 7. Accelerometric data from RERA-4 during free flight.

### 3.2.2. Angular velocity

Figures 8-(a) and 8-(b) show the angular velocity amplitude histories of RERA-2 and RERA-4, respectively. The amplitudes of pitch and yaw were combined into a resultant angular velocity, as shown in equation (2), while the roll angular velocity is shown as raw values. Since the capsule's motion at the moment of release cannot be controlled, RERA-2 exhibited a relatively high roll rate. However, this motion rapidly decayed and stabilized below 10 deg/s. Similarly, RERA-4 showed minimal roll motion, indicating that roll oscillations were not significantly induced by the surrounding flow field for thin aeroshell capsules.

$$w_{xy} = \sqrt{w_x^2 + w_y^2} \tag{2}$$

In contrast, clear differences were observed in the pitch-yaw angular velocities between the two capsules. Although both showed an overall decaying trend, RERA-4 exhibited notably higher angular velocity during the initial 300 seconds after release. These differences will be discussed in detail in

Section 3.2.3 in conjunction with the angle of attack behavior.

The results of a 10-second window FFT analysis applied to the pitch angular velocity are presented in Figure 8-(c). As mentioned previously, the spectrum showed dominant components around 1.3 Hz, which corresponds to the natural oscillation frequency discussed earlier. There were only few peaks found below 0.5 Hz.

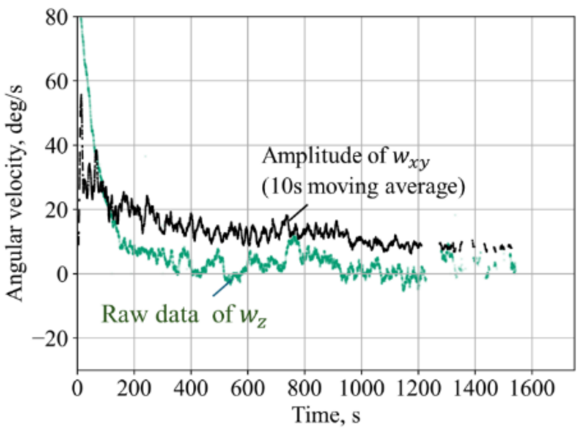


(a) Time history for RERA-2.

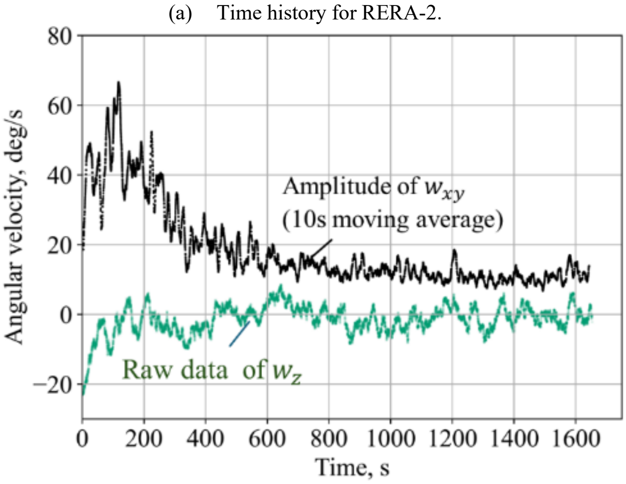


(b) Time history for RERA-4.

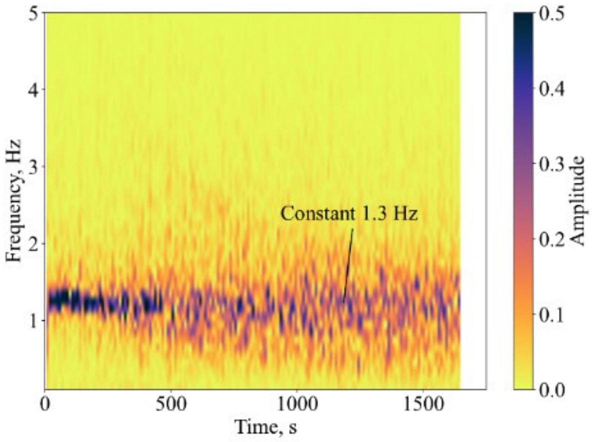


(c) Time history of frequency in pitch for RERA-4.

Fig. 8. Angular velocity data during free flight.

### 3.2.3. Pressure

Figure 9 shows the result of an FFT analysis performed every 10 seconds, along with the differential pressure time history at one of the four measurement points on the front surface of the capsule. The other results of three points had similar trends. The pressure measurement point is indicated in Figure 3, and the recorded value represents the differential pressure relative to the stagnation point. From Figure 9, it can be inferred that two types of oscillations are present: a rotational oscillation around 1.3 Hz and a translational oscillation whose frequency gradually decreases over time.

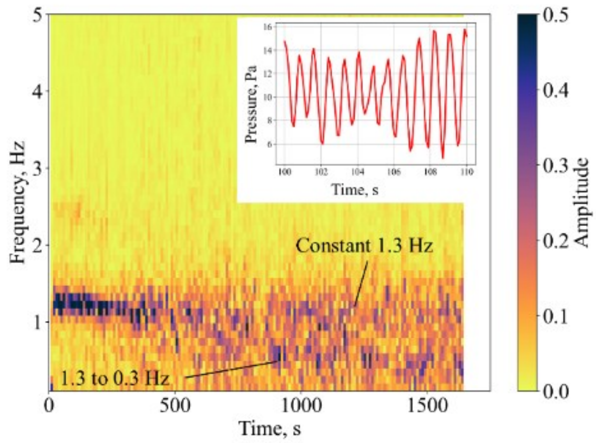


Fig. 9. Time history of FFT analysis for differential pressure history performed every 10 seconds, along with the time history of pressure measured at the front surface of the capsule.

From the pressure distribution at front surface, the angle of attack with respect to the relative wind during free flight can be estimated[12]. As shown in Figure 10, the angles $\theta_{\text{pitch}}$ and $\theta_{\text{yaw}}$ are calculated between the air speed vector and the x-axis in the x-z plane, and the y-axis in the y-z plane, respectively. According to previous studies[13], these angle histories have been successfully obtained and have been shown to qualitatively agree with other data such as acceleration.

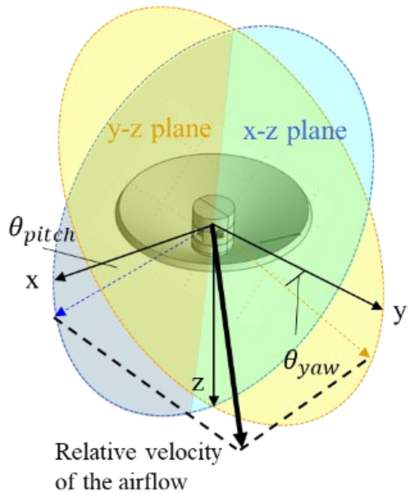


Fig. 10. Definition of angles $\theta_{\text{pitch}}$ and $\theta_{\text{yaw}}$ in the capsule coordinate system.

The capsule's energy is evaluated based on the angle of attack with respect to the relative airflow on each axis and the angular velocity. The generalized energy in rotational oscillation, expressed as the Hamiltonian, is given by Equation (3). Here, p and q are independent variables representing the generalized momentum and generalized coordinate, respectively, as defined in Equation (4). The constant C is used to evaluate the potential energy at a given angular displacement, and in this study, it is defined as the value derived from the static aerodynamic moment about each axis, as shown in Equation (5). Since the capsule is modeled as axisymmetric and the flow-induced rolling moment is assumed to be negligible, $C_z$ is set to zero.

$$H = \frac{p_x^2}{2I_x} + \frac{1}{2}C_x q_x^2 + \frac{p_y^2}{2I_y} + \frac{1}{2}C_y q_y^2 + \frac{p_z^2}{2I_z} + \frac{1}{2}C_z q_z^2 \tag{3}$$

$$p = Iw, q = \theta \tag{4}$$

$$\begin{bmatrix} C_x \\ C_y \\ C_z \end{bmatrix} = \begin{bmatrix} \frac{1}{2}\rho u^2 SDC_{m\alpha} \\ \frac{1}{2}\rho u^2 SDC_{m\alpha} \\ 0 \end{bmatrix} \tag{5}$$

The history of the Hamiltonian was constructed from the angle of attack, angular velocity, and dynamic pressure at each time step. The 10-second moving average of this history is shown in Fig. 11. During free flight, the capsule exchanges energy with the surrounding flow field, and thus the total energy does not remain constant. In the case of RERA-2, the capsule initially lost energy due to the decay of roll motion, and by approximately 200 seconds, the energy reached a nearly constant level. Afterward, the energy decreased gradually, indicating that the capsule flew stably without receiving energy input from the flow in the low-speed regime.

In contrast, RERA-4 exhibited large fluctuations in energy up to around 300 seconds, despite having lower initial energy. It can be observed from the top-right panel of Fig. 11 that a single cycle of energy increase and decrease occurs over approximately 10 oscillation cycles. Previous[6] wind tunnel experiments have shown that subsonic capsules experience chaotic oscillatory behavior in the subsonic regime, similar to that observed in the present flight results. In particular, when the CG is located rearward, as in RERA-4, the amplitude of these oscillations increases[13]. On the other hand, varying the MOI by a factor of two changed the mean oscillation amplitude by at most 20%[10]. Therefore, a 20% change in MOI alone is unlikely to account for the observed differences. Considering these prior findings, it is reasonable to conclude that the increased oscillation in RERA-4 was primarily due to the CG being closer to the aerodynamic center, making the capsule more dynamically unstable.

After 300 seconds, the energy level in RERA-4 decreased to a level comparable to that of RERA-2, indicating a transition to a more stable flight regime. One possible factor contributing to this stabilization is the increase in additional moment of inertia caused by the rise in air density at lower altitudes. Using the flare radius $r$=0.4 m and flare height $h$=0.2 m and multiplying by 2D to account for both the front and rear surfaces of the flare, the additional moment of inertia was estimated as shown in Equation (6). Applying the near-landing air density of 1.3 kg/m$^3$, the additional moment of inertia was approximately 21% of the pitch and yaw MOI for RERA-4. At the time of release, the contribution was approximately 1%. It is suggested that this increases enhanced damping and suppresses the dynamic instability of oscillations.

$$I_{add} = \frac{1}{16}\rho_{air}\pi(r^2 - h^2)^2 \cdot 2D \tag{6}$$

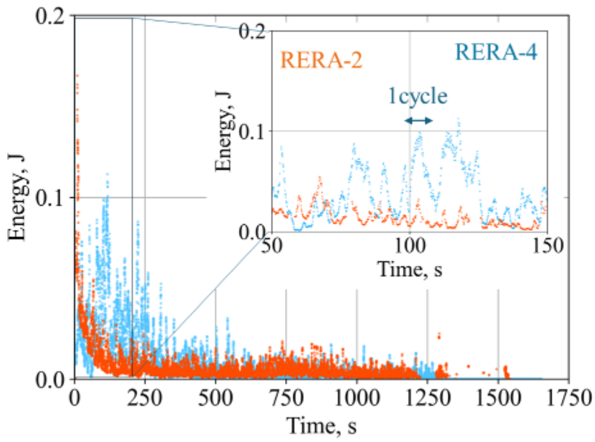


Fig. 11. Time history of Hamiltonian.

## 4. Conclusion

In this study, the free-flight dynamics of the RERA-2 and RERA-4 capsules, which differ in center of gravity (CG) location, were investigated using flight data obtained from balloon drop tests conducted at an altitude of 25 km. Fast Fourier Transform (FFT) analyses of the acceleration, angular velocity, and pressure histories revealed that the dominant frequencies were associated with rotational oscillations driven by static aerodynamic moments and translational oscillations induced by unsteady flow phenomena.

The surface pressure distributions on the capsules were used to estimate the angles of attack relative to the freestream, from which the Hamiltonian representing the oscillatory energy of the capsule was constructed. The Hamiltonian time history for RERA-2 indicated a consistent loss of energy after separation, suggesting that low ballistic coefficient capsules can achieve stable flight in the low-speed regime. In contrast, RERA-4, which had a more aft CG, exhibited large energy fluctuations over approximately ten oscillation cycles. Results from previous 1 degrees-of-freedom wind tunnel tests suggest that this behavior is primarily attributed to the effect of CG position rather than the moment of inertia. Furthermore, as the capsule descended toward the ground, the absence of energy gain indicated that oscillations were suppressed by aerodynamic effects such as the additional moment of inertia due to increasing air density at lower altitudes.

## Acknowledgments

The scientific balloon (DAIKIKYU) flight opportunity was provided by ISAS, Japan Aerospace Exploration Agency (JAXA) (Project ID: BS23-07, BS24-04). This study was supported by JSPS KAKENHI (Grant numbers 20H02360 and 24K01072).

## References

1) Kazuhiko, Y., Toshiyuki, S., Hiroki, T., Takashi, O., Aoi, H., and Tomonari O.: Proposal for Advanced Sample Return Capsule for Deep Space Exploration with Small Spacecraft, Proceeding of 64th Space Sciences and Technology Conference, JSASS-2020-4626-4F02, 2020.
2) Yamada, T. and Yoshihara, K.: Post-flight analysis of recovered components of hayabusa2 sample return capsule, *Journal of Evolving Space Activities*, **1** (2023) p.16.
3) Desai, P. N., Qualls, G. D. and Schoenenberger, M.: Reconstruction of the genesis entry, *Journal of Spacecraft and Rockets*, **45** (2008), no. 1, pp. 33–38.
4) Nagata, Y., Yamada, K., Abe, T. and Suzuki, K.: Attitude dynamics for flare-type membrane aeroshell capsule in reentry flight experiment, in AIAA Aerodynamic Decelerator Systems (ADS) Conference.
5) Kazemba, C. D., Braun, R. D., Clark, I. G. and Schoenenberger, M.: Survey of Blunt-Body Supersonic Dynamic Stability, *Journal of Spacecraft and Rockets*, **54** (2017), no.1, pp.109-127.

}

}

6) Hiraki, K.: Experimental study on dynamic instability of capsule-shaped body, *ISAS Rep.*, **103** (1999), pp. 1–55.
7) Takasawa, H., Fujii, T., Takahashi, Y., Moriyoshi, T., Takayanagi, H., Nagata, Y. and Yamada, K.: Static attitude stability of deep space sample return capsule with thin aeroshell, *CEAS Space Journal*, **17**(2025), pp.55-69.
8) The global forecast system, the national centers for environmental prediction (NCEP), 1997, https://www.ncei.noaa.gov/products/weather-climatemodels/global-forecast (accessed July 06, 2024).
9) Schoenenberger, M., Norman, J.V., Karlgaard, C., Kutty, P., and Way.: Assessment of the reconstructed aerodynamics of the Mars science laboratory entry vehicle, *J. Spacecraft and Rockets*, **4** (2014), 51, 1076-1093.
10) Takasawa, H.: Study of Aerodynamic Instability for Reentry Capsule with Thin Aeroshell, Ph.D. Thesis, Hokkaido University, 2024.
11) Berger, E., Scholz, G. and Schumm, M.: Coherent vortex structures in the wake of a sphere and a circular disk at rest and under forced vibrations, *Journal of Fluids and Structures*, **4** (1990), no. 3, pp. 231–257.
12) Wickens, R. and Williams, C.: Calibration and use of five-hole flow direction probes for low speed wind tunnel application, Scientific and Technical Publications AD-A160-262, National Aeronautical Establishment, 1985.
13) Yoshio, T.: The Effect of Center of Gravity on Attitude Instability of Reentry Capsule with thin Aeroshell at Subsonic Speed, Master's thesis, Hokkaido University, 2024.